Geocarto International
Publication details, including instructions for authors and subscription information:
http://www.tandfonline.com/loi/tgei20

Risk assessment of soil erosion in semi-arid mountainous watershed in Saudi Arabia by RUSLE model coupled with remote sensing and GIS

Javed Mallick[a], Yasser Alashker[ab], Shams Al-Deen Mohammad[ac], Mohd Ahmed[a] & Mohd Abul Hasan[ad]

[a] Faculty of Engineering, King Khalid University, Abha, Kingdom of Saudi Arabia

[b] Faculty of Engineering, Zagazig University, Ash Sharqiyah, Egypt

[c] Faculty of Engineering, Banha University, Qalyubia, Egypt

[d] Faculty of Engineering, Jamia Millia Islamia, New Delhi, India

Accepted author version posted online: 17 Jan 2014.Published online: 14 Feb 2014.

To cite this article: Javed Mallick, Yasser Alashker, Shams Al-Deen Mohammad, Mohd Ahmed & Mohd Abul Hasan , Geocarto International (2014): Risk assessment of soil erosion in semi-arid mountainous watershed in Saudi Arabia by RUSLE model coupled with remote sensing and GIS , Geocarto International, DOI: 10.1080/10106049.2013.868044

To link to this article: http://dx.doi.org/10.1080/10106049.2013.868044

Geocarto International, 2014
http://dx.doi.org/10.1080/10106049.2013.868044

Taylor & Francis
Taylor & Francis Group

Risk assessment of soil erosion in semi-arid mountainous watershed in Saudi Arabia by RUSLE model coupled with remote sensing and GIS

Javed Mallick[a]*, Yasser Alashker[a,b], Shams Al-Deen Mohammad[a,c], Mohd Ahmed[a] and Mohd Abul Hasan[a,d]

[a]*Faculty of Engineering, King Khalid University, Abha, Kingdom of Saudi Arabia;* [b]*Faculty of Engineering, Zagazig University, Ash Sharqiyah, Egypt;* [c]*Faculty of Engineering, Banha University, Qalyubia, Egypt;* [d]*Faculty of Engineering, Jamia Millia Islamia, New Delhi, India*

(*Received 16 September 2013; final version received 28 October 2013*)

Soil erosion is the most important factor in land degradation and influences desertification in semi-arid areas. A comprehensive methodology that integrates revised universal soil loss equation (RUSLE) model and GIS was adopted to determine the soil erosion risk (SER) in semi-arid Aseer region, Saudi Arabia. Geoenvironmental factors viz. rainfall (R), soil erodibility (K), slope (LS), cover management and practice factors were computed to determine their effects on average annual soil loss. The high potential soil erosion, resulting from high denuded slope, devoid of vegetation cover and high intensity rainfall, is located towards the north western part of the study area. The analysis is investigated that the SER over the vegetation cover including dense vegetation, sparse vegetation and bushes increases with the higher altitude and higher slope angle. The erosion maps generated with RUSLE integrated with GIS can serve as effective inputs in deriving strategies for land planning/management in the environmentally sensitive mountainous areas.

Keywords: soil erosion; semi-arid watershed; RUSLE model; geospatial techniques

1. Introduction

Soil erosion is the most important factor in land degradation and influences environmental problem worldwide (Fernandez & Nunez 2011). In mountainous environments soil erosion often constrains local development and exacerbates poverty by undermining the productive capacity of highland farming and livestock raising (Zimmerer 1993; Lal 2001; Alewell et al. 2008). Field studies for prediction and assessment of soil erosion are neither cost effective nor time effective. Despite the fact that providing detailed understanding of the soil erosion processes, field studies have limitations because of geographical complexity of interactions and the difficulty of generalizing from the results (Saha & Pande 1993). Soil erosion models integrated with GIS can simulate erosion processes in the watershed altogether of the complex interactions that affect rates of erosion.

Soil erosion dynamic is influenced by spatial heterogeneity such as elevation, vegetation cover, soil properties and land use/land cover (LULC), etc. Soil erosion estimation and prediction is relevant at a wide range of spatial scales, from the large scale to

*Corresponding author. Email: jmallick@kku.edu.sa

the catchment scale, from the regional scale up to the continental and global scales (Vrieling 2006). Soil erosion at different scales and various processes tends to become dominant, so in this case the effective focus of the models also changes. Soil erosion at the larger scales, topography, soil properties and vegetation covers becomes more important (Bonilla et al. 2010). This is where remote sensing (RS) and GIS become more valuable and useful tools.

The advantages of linking soil erosion models with a RS and GIS are the possibility of rapidly producing input data to simulate different soil erosion scenarios, ability to use very large catchments area (De Roo 1996), areas can be simulated at a user-defined resolution (Xia & Clarke 1997; Qinke et al. 2002; Renschler & Flanagan 2002) and visualization can be used to display and animate a sequence of model output across time and space. Various studies have shown the potential use of RS and GIS in soil erosion mapping in combination with soil, rainfall, vegetation cover and topography information (Narayana & Babu 1983; Dwivedi et al. 1997; Hill & Schütt 2000; Fu et al. 2005; Metternicht & Gonzalez 2005; Dabral et al. 2008; Kouli et al. 2009; Bonilla et al. 2010; Hasan et al. 2013).

Ayed and Adam (2010) investigated the effects of different vegetation types on run-off generation and soil erosion. In this it was concluded that the run-off and soil erosion were found to be more reduced based on the type of vegetative cover rather than the per cent of vegetative cover. Fattet et al. (2011) suggested that combination of different plant functional types would improve soil conservation on slopes, by reducing both surface water erosion and shallow substrate mass movement.

Since the 1930s', soil erosion assessment and prediction has been a challenge to researchers (Lal 2001). Numerous soil erosion models have been developed, viz. the Water Erosion Prediction Project (WEPP) model (Nearing et al. 1989), the Chemical, Runoff, and Erosion for Agricultural Management System (Knisel 1980), the European Soil Erosion Model (Morgan et al. 1990), etc. Among these models, revised universal soil loss equation (RUSLE) is one of the most widely used model (Wischmeier & Smith 1978; Renard et al. 1997; Lee & Lee 2006; Yuksel et al. 2008; Adediji et al. 2010; Prasannakumar et al. 2012), and has been applied in areas of different spatial scales and environmental conditions (Angima et al. 2003; Cohen et al. 2005; Prasannakumar et al. 2012). The RUSLE model is very efficient, robust and simple, although it suffers from a number of drawbacks concerning extrapolation, spatial scale effects and the complexity of the entire soil erosion process (Li et al. 2011).

A thorough literature survey shows that no significant research has been conducted for the potential soil erosion risk (SER) and its impact on sustainability in semi-arid mountainous watershed of Abha. With the above background, this study evaluates the annual SER and developed a potential soil erosion map for a semi-arid watershed using RUSLE model integrated with GIS. The resultant map can be used as scalable model for various watersheds in similar semi-arid settings and the variation of erosion with reference to different LULC practices.

2. Study area and material used

2.1. Study area

The semi-arid Abha mountainous watershed is situated in Aseer province of kingdom of Saudi Arabia (Figure 1). It covers an area of 370 km^2. The boundary of the study area lies between the latitude 18°10′12.39″N and 18°23′33.05″N and longitude 42°21′41.58″E

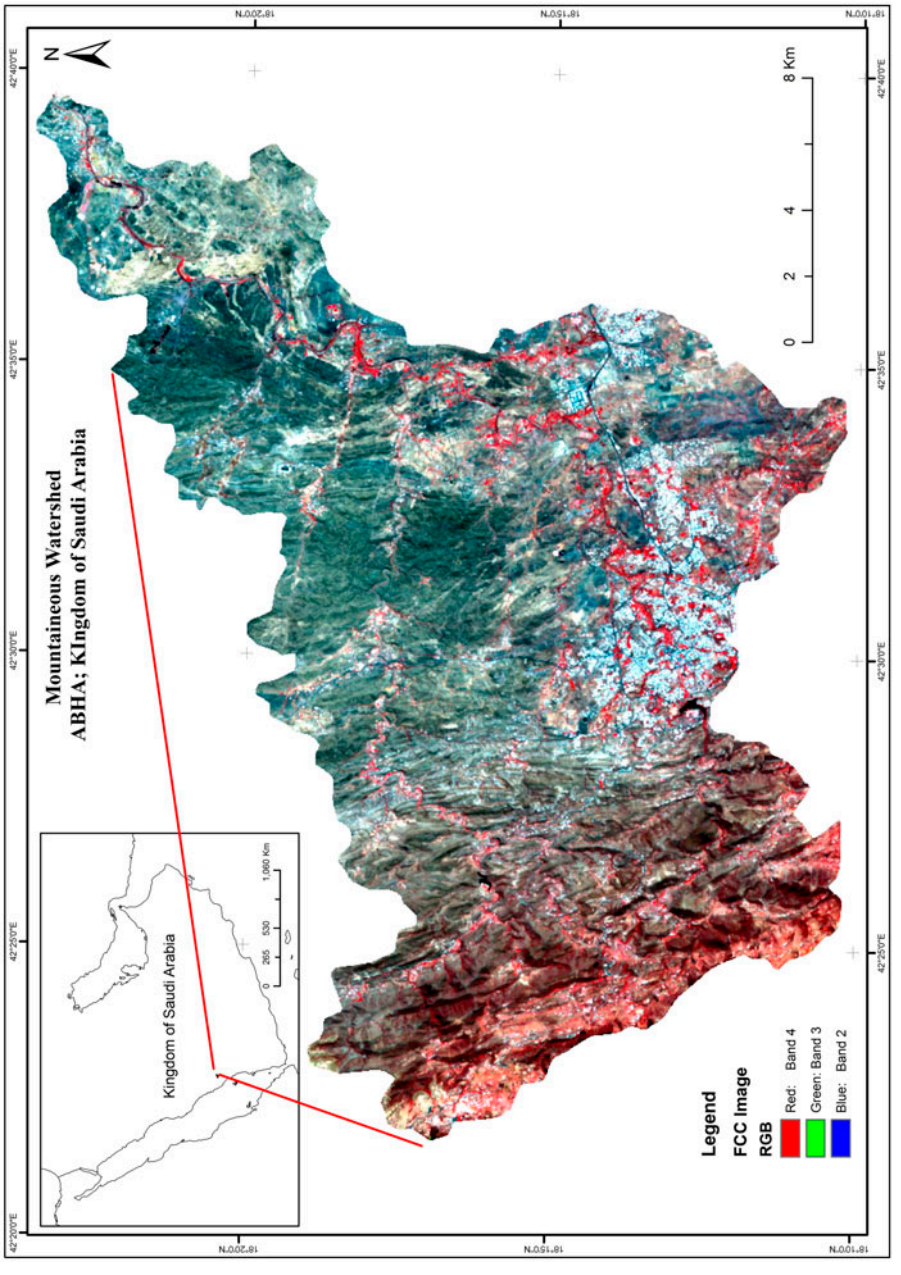

Figure 1. Study area.

and 42°39′36.09″E. The topography of the area is undulating and the elevation ranges from 1951 to 2991 m mean sea level. The average annual rainfall of 355 mm with the bulk of the precipitation is occurring between June and October and average minimum and maximum temperatures of 19.3° and 29.70 °C, respectively. The study area embraces one of the richest and the most variable floristic regions of Aseer Mountains, south-west of Saudi Arabia. Jabal Al-Sooda, located in the north western part of the watershed area, 2991 m high, has also a rich flora. The variation in climate and topography in the study area (Aseer Province) has led to the formation of diverse plant community (Abulfatih 1981). As per the geological setting (Faulkender 1984) of the study area, analysis of topography (Digital Elevation Model, DEM) and rainfall pattern for the last decade, it is concluded that the area has severe problem of soil erosion thus affecting the productivity of agriculture and forestlands.

2.2. *Materials*

The data-set used in the study is given in Table 1. All data have been converted into raster at 15 m cell size, so that spatial analysis can be done in the same cell size and map projection. Garmin-38s GPS navigator has been used for field survey to collect the GCPs.

3. Methodology

General approach of this study is to ascertain the SER. A general approach for the methodology is described in Figure 2.

3.1. *Reconnaissance survey and laboratory analysis*

Reconnaissance survey was carried out during March–April month of 2013 to collect soil samples for texture analysis. A total of 75 soil samples, approximately 1 kg, (at the depth of 0–30 cm) were collected from the study area for aggregate stability . The soil sampling was done using stratified composite approach, i.e. the region is subdivided into areas of similar topography, soil moisture and LULC. Thereafter, this area is then

Table 1. Data-sets.

Subject area	Data basis	Source
Basic data	Administrative boundaries flowing wadies, village and its boundary	MOMRA, KSA
Precipitation data	Monthly precipitation data from 4 rainfall stations from 2001 to 2010	Presidency meteorological environment (PME) KSA
Soil data	General soil class; Soil characteristics (% silt, sand and clay) and organic contents	Ministry of agricultural, ABHA, KSA; Extensive field survey/ Laboratory analysis
Satellite data used for LULC and vegetation cover	ASTER (15 Nov. 2010) Path/Row = 167/47–48	TERRE/ASTER NASA
Topographical data	Contour line, spot height, DEM, Mean slope; mean slope exposure	MOMRA, KSA
Geological map	Geological unit	Saudi geological survey, KSA

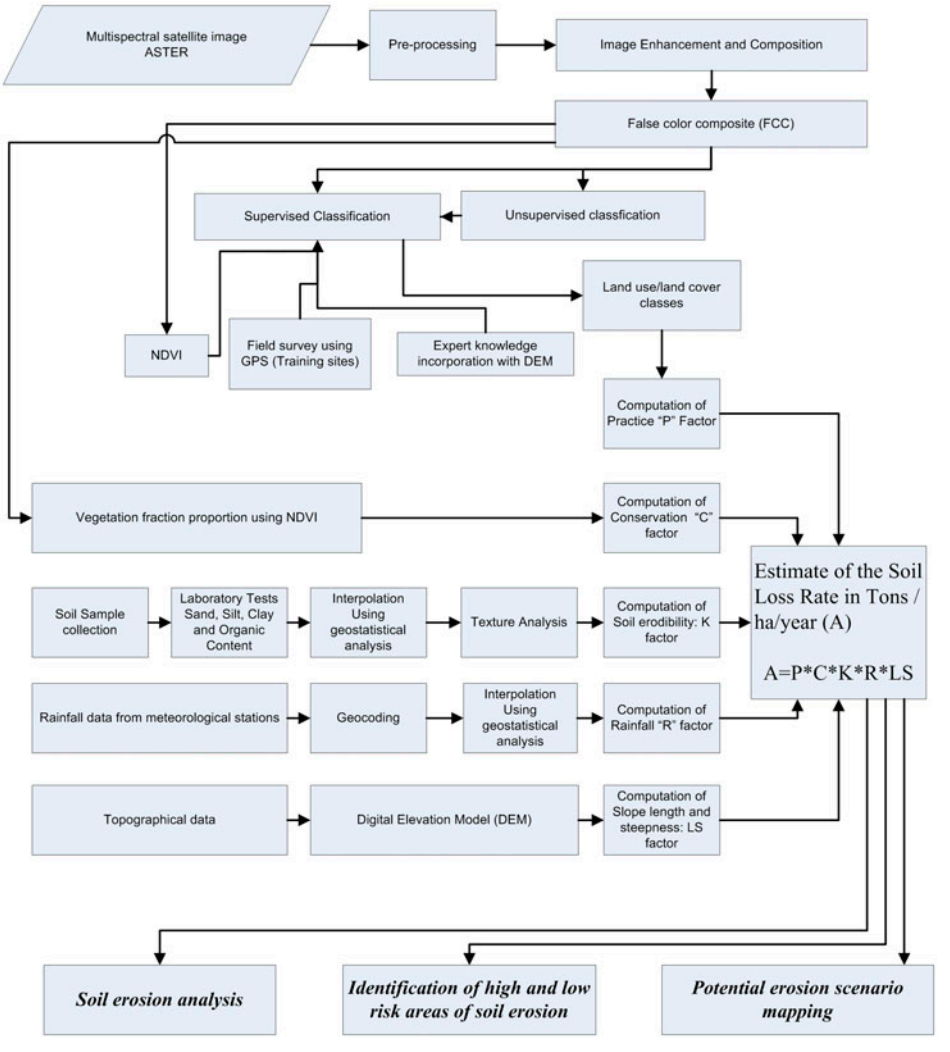

Figure 2. Flow chart risk assessment of soil erosion using RUSLE coupled with geoinformation technology.

sampled separately and at each survey location, two replicates, 2–3 m apart were collected. Individual samples were weighed and carefully sieved through a 2 mm screen and later analysed in laboratory for their soil grain properties, namely soil texture and organic matter, using standard procedure described by Carter (1993).

3.2. *Hydrometer method for soil texture*

The hydrometer method is based on the change of density of a soil and water suspension upon the settling of the soil particles. For the soil dispersion sodium hexametaphosphate, $(NaPO_3)_6$ was used. Stokes' Law is used to predict the settling times for various sized particles. Stokes' law states that the rate which particles fall in a viscous

medium (water) is governed by the radius of the particles and the force due to gravity. A special hydrometer, calibrated in terms of the grams of soil suspended, is used to measure density. The hydrometer is gently placed into the cylinder containing the suspension after predetermined periods of time and a reading is taken by determining where the meniscus of the suspension strikes the hydrometer.

3.3. Soil properties: interpolation

The soil texture and organic matter content of topsoil were used to calculate the K factor at 15 m pixel size. A data-set of soil properties was created with their georeferenced position in the field. Different digital maps of the soil properties are created to understand the variation of the erodibility factors, using geostatistics tools. Figure 2 shows all the factors needed to estimate SER and underline the aim of this study, the soil erodibility factor and properties needed according RUSLE. Before creating surface diagrams, the distribution of the different soil properties is analysed using geostatistical tool to better understand the trends, influences directional and obvious errors. Transformation and trend removal was performed. Ordinary kriging was used and semi-variograms, which expresses the spatial dependence between neighbouring observations, were produced for each soil factor. Kriging cross-validation was used to estimate that the semi-variogram models could give the most accurate predictions of the unknown values of the field. The closer the mean error was to zero and the closer the root-mean-square standardized error was to 1 signify that the prediction values were close to measured values. The models which presented similar values for mean error and root-mean-square error, the lowest values of root-mean-square error and average standard error were taken into consideration. Thereafter, all maps of soil properties, which resulted from the interpolation techniques, were reclassified.

3.4. Topographical data

Topography is one of the prime inputs to any soil erosion and hydrological modelling, since it defines the effect of gravity on the movement and flow of water and sediments. LS (length and slope) factor can be estimated from a DEM (Hickey 2000; Boggs et al. 2001; Gertner et al. 2002; Wang et al. 2003; Remortel et al. 2001; Hasan et al. 2013). The process of DEM creation begins with the scanned, georeferenced Topographic Map or raster image (1:50,000). Contour Lines with 25 m interval, spot elevations, from the raster image are extracted, converted to digital vectors and given elevation (height) values from topographic sheets. The Grid-based DEM was generated from the extracted digital contour vector data. The DEM was produced with the 'Topo to Raster' interpolation techniques in 3D Analyst tool of ArcGIS 10.1. 'Topo to Raster' is an interpolation techniques specially designed for the creation of hydrologically corrected DEM (Hutchinson 1989; Hutchinson & Dowling 1991). The range of elevation of the watershed is found to be from 1951 to 2991 m. The maximum height shows towards the western part of watershed whereas it gradually decreases towards the eastern part the watershed.

3.5. Digital image classification

Land cover data assist in improving the representation of physical land processes and supervised classification was used as a technique to categorize the image into different

LULC categories. Supervised classification can be used to cluster pixels in satellite data-set into classes corresponding to user-defined training classes. This classification type requires selecting training areas for use as the basis for classification. The most common supervised classification technique is the maximum likelihood classifier for parametric input data and parallelpiped classifier for non-parametric data (Lillisand & Keifer 2000). Accordingly, representative points expected to represent the various land cover classes were marked using GPS during the field visit for the accessible places. These points were used to sample representative signatures for the various land cover types identified during the field visit. Following this, supervised LULC classification has been carried out using ILWIS software (open source). Considering the objectives of the present study, Anderson et al. (1976), LULC classification scheme have been adopted as follows: built-up land, dense vegetation (forest), sparse vegetation (including parks), water bodies, fallow land, waste land/bare soil, agricultural cropland, exposed rocks and scrubland and bushes.

The Figure 3 shows the LULC of 2010, the most dominant class in 2010 was the rock exposed land (51.50%) followed by bushes and scrubland 10.97%, sparse vegetation (10.46%) and agricultural cropland 4.31% (Table 3). The built-up area is mainly in the central, south eastern part of the study area. This transformation may be connected to the change in the economic base of the city from agriculture to secondary activities. The overall accuracy of LULC map of 2010 was 88.35 and Kappa coefficient was 0.866. The user's accuracy in some of the class's viz., built up and agricultural cropland classes, etc. is found relatively low. This is attributed to intermixing in the classes in different altitudinal zones, uncertainty in spectral reflectance in features class. Some of the class's viz. waterbodies, fallow land and rock exposed showed a very good agreement.

3.6. *Vegetation fraction cover*

Vegetation cover is the second most important factor that controls SER. The vegetation-related parameters, which account for the protection given by the canopy cover and ground cover. Accurate information about the spatial distribution of the fraction vegetation cover types is hence of utmost importance. In the RUSLE, the effects of vegetation cover are incorporated in the cover management factor (*C* Factor). It is defined as the ratio of soil loss from land cropped under specific conditions to the corresponding loss from clean-tilled, continuous fallow (Wischmeier & Smith 1978). The value of *C* mainly depends on the vegetation's cover percentage and growth stage. In the present study, an attempt has been made by taking the proportion of vegetation cover per pixel. The proportions of vegetation cover for each pixel through satellite data is calculated using (Equation (1)), the following relation (Valor & Caselles 1996; Mallick et al. 2008):

$$P_V = \frac{(1 - i/i_g)}{(1 - i/i_g) - k(1 - i/i_v)} \tag{1}$$

where

i_g = NDVI value of pure soil pixel
i_v = NDVI value of pure vegetation pixel
$k = (\rho_{2v} - \rho_{1v})/(\rho_{2g} - \rho_{1g})$.

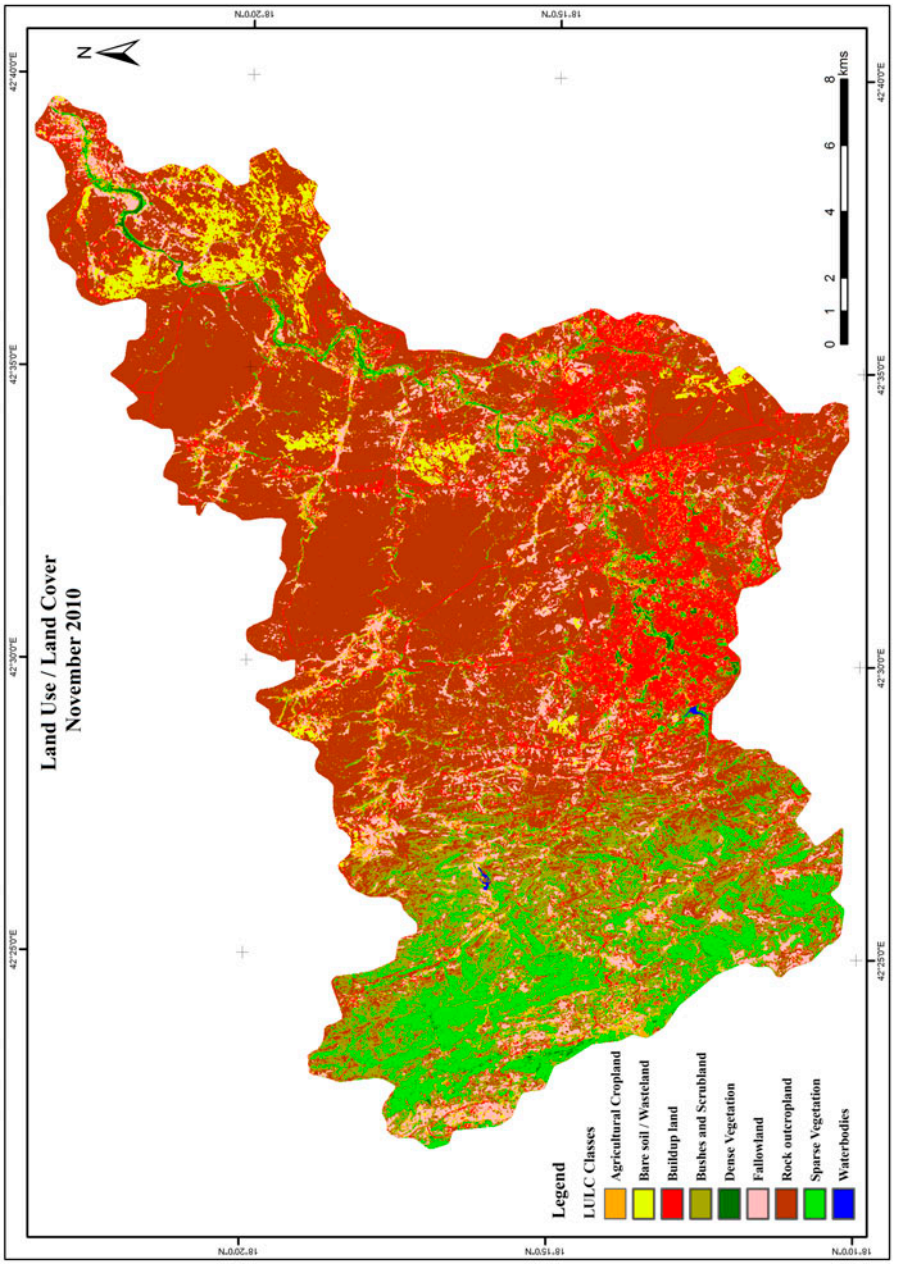

Figure 3. LULC, derived from ASTER satellite data-sets 2010.

where ρ_{2v} and ρ_{1v} are reflectance in the NIR and red region for pure vegetation pixels; $\rho_{2\,g}$ and $\rho_{1\,g}$ are the reflectance in the NIR and red region for pure soil pixels respectively; and 'i' is the NDVI value of mixed pixels. The application of the model has two parts. For the first part, the vegetation and bare soil proportions are obtained from the NDVI of pure pixels.

3.7. *Soil erosion model structure*

Considering the available data, the size of the watershed and the purpose of the study, the RUSLE model (Renard et al. 1997) was chosen to assess the erosion risk. It is designed to predict the long-term average annual soil loss using RUSLE by the following Equation (2):

$$A(i,j) = R(i,j) \times LS(i,j) \times K(i,j) \times C(i,j) \times P(i,j) \tag{2}$$

where A is the estimated average annual soil loss per unit area per year (t $ha^{-1}\,y^{-1}$). Data preparation required to run above-mentioned algorithm is given below:

- Estimation of rainfall erosivity factor (R) (MJ mm $ha^{-1}\,h^{-1}\,y^{-1}$) of a grid located at (i, j).
- Estimation of LS, the slope length and steepness factor, is the average topographical parameter of a grid located at (i, j).
- Estimation of K is the average soil erodibility factor (t ha h $ha^{-1}\,MJ^{-1}\,mm^{-1}$) of a grid located at ($i$, j).
- Estimation of C is the cover management factor of a grid located at (i, j).
- Estimation of P is the conservation management practice factor of a grid located at (i, j).

3.7.1. *Rainfall erosivity (R)* factor

The rainfall erosivity factor, an index unit, is a measure of the erosive force of a specific rainfall. This is determined as a function of the volume, intensity and duration of rainfall and can be computed from a single event, or a series of events to include cumulative erosivity from any time period. Raindrop erosion is the dominant type of soil erosion in barren soil surfaces. For computing this factor, it needs the rainfall intensity observations in the study area. It estimates the R factor with sufficient long-term observations of the rainfall intensity in the area. In the present study, rainfall data of 10 years (2001–2010) collected from Presidency of Meteorological Environment KSA were used for calculating R-factor using the Equation (3) developed by Wischmeier and Smith (1978) and modified by Arnoldus (1980):

$$R = \sum_{i=1}^{12} 1.735 \times 10^{\left(1.5 \log_{10}\left(\frac{P_i^2}{P}\right) - 0.08188\right)} \tag{3}$$

where

R is the rainfall erosivity factor (MJ mm $ha^{-1}\ h^{-1}\ y^{-1}$)

P_i is the monthly rainfall (mm) and

P is the annual rainfall (mm).

For the present study, R-factor was computed from four available meteorological stations data (namely Abha, Khamish Mushayet, Al-Sooda and Bisha), for rainfall

intensity. IDW interpolation technique (Lu & Wong 2008) was used along with rainfall data from stations for assessing the spatial variability in the rainfall and rainfall erosivity in the study area. In order to make the *R*-factor value most reliable, the spatial distribution of *R* was calculated from the available rainfall data by considering that the area experiences relatively uniform rainfall, both in intensity and duration across the study area and the average *R* value was used for further calculation (Table 2). During 2001–2010, the rainfall erosivity was found to be in the range of 133.74–549.68 MJ mm ha ha^{-1} h^{-1} y^{-1}. The average *R*-factor was observed to be 234.14 MJ mm ha^{-1} h^{-1} y^{-1}. The highest value (684.53 MJ mm ha^{-1} h^{-1} y^{-1}) of *R*-factor was observed in 2004 and the lowest value (56.47 MJ mm ha^{-1} h^{-1} y^{-1}) was in 2009. Figure 4 shows the spatial distribution of rainfall erosivity of 2001–2010.

3.7.2. *Slope length and steepness: LS factor*

The effect of topography on soil erosion in RUSLE is accounted for by the *LS* factor. It contains two subcomponents: the length factor (*L*) and the steepness factor (*S*) (Renard et al. 1997; Lu et al. 2004). The slope length and steepness derived from the DEM depend on the spatial resolution. Hence, for accurate estimates of slope length and angle, a high-resolution DEM is a prerequisite.

The effect of topography on soil erosion in RUSLE has two components, the length factor (*L*) and the steepness factor (*S*). Mitasova et al. (1996, p. 630) computed the LS-factor as proposed by Wischmeier and Smith (1978) as in Equation (4).

$$LS = \left(\frac{\lambda}{22.13}\right)^{m} \times (65.4\sin^2\beta + 4.56\sin\beta + 0.0654) \tag{4}$$

where:

λ = the slope length (m), it is defined as the horizontal distance from the original of overland flow to the point where deposition begins or where run-off flows into a defined channel.

m = the length exponent dependent on the value of the slope,

β = The slope angle (β)

So, slope length λ is calculated (Desmet & Govers 1996) using Equation (5)

$$L(i,j) = \frac{(A(i,j) + D^2)^{m+1} - A(i,j)^{m+1}}{x^m \times D^{m+2} \times (22.13)^m} \tag{5}$$

where m value calculated from Equation (6)

$$m = \frac{F}{1+F}; \quad F = \frac{\sin\beta/0.0896}{3(\sin\beta)^{0.8+0.56}} \tag{6}$$

Slope angle β is taken to be the mean angle of all subgrids in the steepest direction, (McCool et al. 1989) Equation (7)

$$S(i,j) = \left\{ \begin{array}{l} 10.8\sin\beta(i,j) + 0.03, \tan\beta(i,j) < 0.09 \\ 16.8\sin\beta(i,j) - 0.50, \tan\beta(i,j) \geq 0.09 \end{array} \right\} \tag{7}$$

Figure 4 shows the spatial distribution of LS factor. The LS factor value in the study area varies from 0.03 to 31.528, with mean and standard deviation of 15.78 and 9.09, respectively.

Table 2. Monthly rainfall data with annual average rainfall erosivity (*R*) factor.

Monthly rainfall data with annual average *R*-factor (MJ mm ha^{-1} h^{-1} y^{-1})																	
	Months												*R*-factor				
Year	1	2	3	4	5	6	7	8	9	10	11	12	Min	Max	Std.	Avg.	10 Yr. Avg. *R*
2001	1.4	0.0	21.7	3.1	8.4	34.1	20.3	46.8	11.9	45.9	0.0	1.3	98.6	375.5	80.3	168.6	Min: 133.74
2002	17.6	18.2	10.2	21.9	24.9	33.3	6.8	13.7	19.6	2.8	7.0	30.1	33.7	222.8	52.4	81.1	Max: 549.68
2003	0.0	16.8	0.0	16.6	9.4	4.1	9.7	25.2	7.2	0.0	0.0	0.6	44.7	51.0	1.7	46.9	STD. 114.99
2004	2.6	6.3	11.5	69.6	39.1	37.8	20.6	17.3	96.6	0.5	0.3	2.3	325.5	1654.5	341.1	684.5	Avg. *R*: 234.14
2005	26.1	0.0	1.0	34.3	74.4	22.2	13.5	54.0	49.1	0.0	0.2	60.9	142.8	804.7	189.2	309.2	
2006	0.0	0.0	2.6	49.5	32.5	15.5	29.5	58.4	37.8	1.0	0.4	0.1	174.3	566.0	100.7	291.2	
2007	5.4	12.4	0.8	30.3	9.3	31.7	7.6	11.5	26.2	8.2	2.2	15.8	56.6	162.4	27.9	79.6	
2008	7.3	10.4	16.3	7.2	40.8	15.5	13.7	62.7	17.8	4.0	11.0	10.9	59.0	598.5	163.4	200.1	
2009	4.9	8.5	0.9	11.0	13.9	23.5	9.6	26.7	17.6	0.0	4.8	5.9	18.2	156.4	40.7	56.5	
2010	0.0	5.0	2.3	11.9	26.2	60.5	91.6	69.0	10.6	7.8	11.8	0.2	192.0	905.1	205.6	423.2	

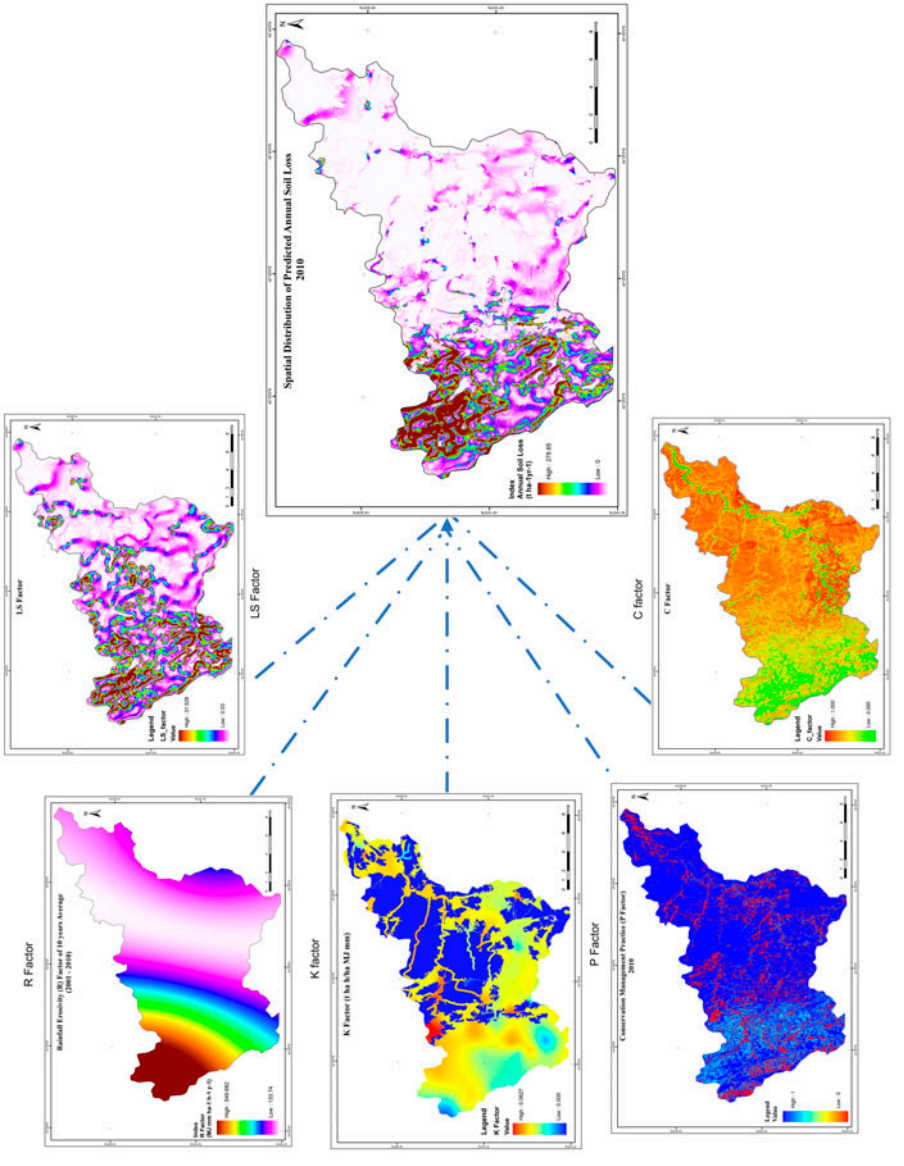

Figure 4. Annual average soil loss map of semi-arid mountainous watershed, 2010.

3.7.3. Soil erodibility factor (K)

K factor is soil erodibility factor, which represents both susceptibility of soil to erosion and the rate of run-off. Specifically, the k factor is a function of grain size, drainage potential, soil structural integrity, organic content, cohesiveness structure and permeability (Renard et al. 1997; Prasannkumar et al. 2012). In this study area, Equation (8) was used to calculate K value recommended by Wischmeier and Smith (1978).

$$K = 0.0293(0.65 - D_G + 0.24D_G^2)\exp\left\{-0.0021\left(\frac{OM}{f_{\text{clay}}}\right) - 0.00037\left(\frac{OM}{f_{\text{clay}}}\right)^2 - 4.02f_{\text{clay}} + 1.72f_{\text{clay}}^2\right\} \quad (8)$$

where

The geometric mean of particle size, and K is in (t ha h $\text{ha}^{-1}\,\text{MJ}^{-1}\,\text{mm}^{-1}$), OM is percentage of organic contents, f_{sand} is the fraction of sand (particle size of 0.05 – 2.0 mm), f_{silt} is the fraction of silt (particle size 0.002 – 0.05 mm) and f_{clay} is the fraction of clay (particle size less than 0.002 mm). D_G was calculated from Equation (9)

$$D_G = -3.5f_{\text{clay}} - 2.0f_{\text{clay}} - 0.5f_{\text{sand}} \quad (9)$$

Figure 5 shows the sand, silt, clay and organic contents. Figure 4 shows the spatial distribution of K factor. The K factor value in the study area varies from 0.000 to 0.0627 t ha h $\text{ha}^{-1}\,\text{MJ}^{-1}\,\text{mm}^{-1}$, with mean and standard deviation of 0.043 and 0.0147, respectively. Figure 4 shows the spatial distribution of the K factor and it is inferred from the map that the highest values are located towards the north western part of the study area.

3.7.4. Cover management factor (C)

The cover management factor (C) was calculated from fraction vegetation cover data using the Equation (10), recommended by Renard et al. (1997) for the data-sets of 2010.

$$CC = 1 - F^c \times \exp(-0.03045 \times H) \quad (10)$$

where CC is the canopy cover sub factor range from 0 to 1, F_c is fraction of land surface covered by canopy and H (m) is distance that raindrops fall after striking the canopy. For the former, we used the average weighted tree height 5.8 m (an extensive field survey has been conducted to estimate the average height of acacia species that is prevalent in the region), (Handbook of Arabian medicinal herbs, 2009) and for the latter, the estimated shrub and grass height 0.5 m was used. Figure 4 shows the C factor map, value ranges from 0.125 to 1.00 with the mean and standard deviation of 0.949 and 0.076, respectively.

3.7.5. Conservation management practice factor (P)

The P values range from 0 to 1, 0 represents a very good manmade erosion resistance facility, and value 1 represents no manmade resistance erosion facility. The P factors indicate the effect of land use, agricultural and erosion conservation practices on the annual soil loss from the watershed. RUSLE uses the P factor for support practices (Renard et al. 1997). The values of P factor are related to the land use identified by

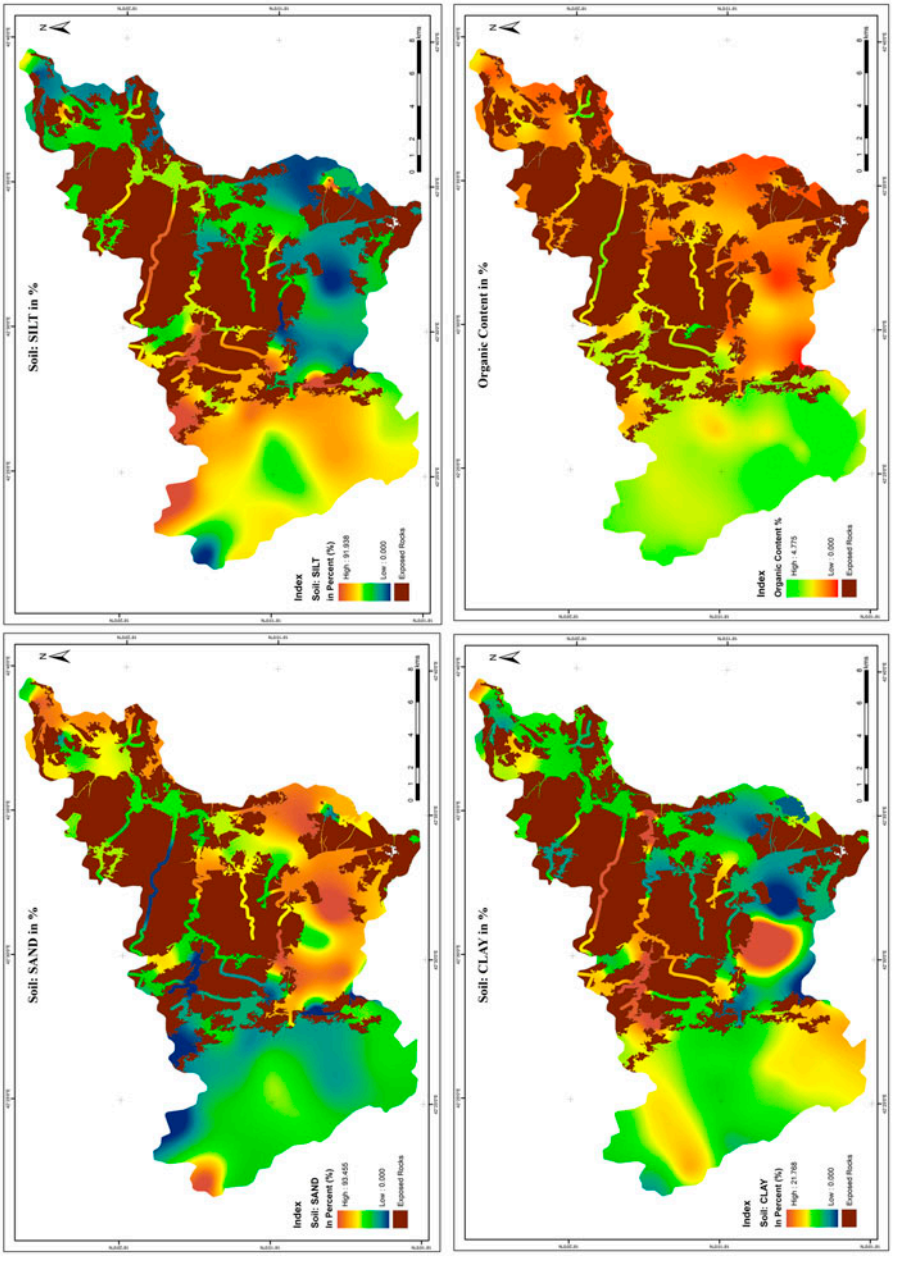

Figure 5. Soil properties map (sand, silt, clay and organic content).

Table 3. *P* factors for different land cover types.

Sl. No.	LULC classes	Surfaces 2010		*P* factor
		Area in km	%	
1	Build-up land	35.57	9.61	1.0
2	Water bodies	0.12	0.03	0.0
3	Agricultural cropland	15.94	4.31	0.5
4	Dense vegetation	2.04	0.55	1.0
5	Sparse vegetation	38.69	10.46	1.0
6	Fallow land	31.76	8.58	0.5
7	Bare soil/wasteland	14.76	3.99	1.0
8	Bushes and scrubland	40.60	10.97	0.8
9	Rock exposed	190.55	51.50	1.0
	Total	370	100.00	

land cover types. Table 1 below shows the average values for *P* for each land cover type taken from Wischmeier and Smith (1965).The *P* factor in RUSLE is the ratio of soil erosion with a specific support practice to the corresponding soil loss with straight-row upslope and down slope tillage. The *P* factor accounts for control practices that reduce the erosion potential of the run-off by their influence on drainage patterns, run-off concentration, run-off velocity and hydraulic forces exerted by run-off on soil (Renard et al. 1997). Human knowledge on soil erosion control is important to include in the *P* factor, but there is no reliable reference available for the study area. Hence, a *P* factor is calculated on the basis of LULC and assigned the weight as per the USDA (Table 3). Figure 4 shows the *P* factor map of the study area.

4. Results and discussion

RUSLE is an empirical-based model that has the ability to predict long-term average annual soil erosion rate using rainfall pattern, soil properties, topography, vegetation proportion cover and management practices. In the present research, annual soil erosion rate map was generated for Abha watershed, a mountainous area, which represents most of the terrain characteristics of Aseer region, Saudi Arabia. Several data sources were used for the generation of RUSLE model inputs (*R*, *K*, LS, *C* and *P*) factors and stored as raster layers in the ArcGIS software. Potential soil erosion is estimated using RUSLE model, which represents geoenvironmental scenario of the study area.

4.1. Average annual soil erosion rate

Figure 4 shows the average soil erosion rate map of 2010, estimated for the Abha watershed, which ranges from 0 to 278.65 t h^{-1} y^{-1} with standard deviation of 34.91t h^{-1} y^{-1}. The results were compared with the studies carried out in areas having similar (Matsuura 2000; Bacchi et al. 2000; Mati 2000; Shiono et al. 2002; Angima et al. 2003; Lee & Lee 2006; Yuksel et al. 2008; Adediji et al. 2010; Prasannakumar et al. 2012) geoenvironmental and rainfall characteristics and were found to be comparable with an annual average soil erosion rate of 16.10 t h^{-1} y^{-1}. The figure shows pattern of the potential soil risk area. The high soil erosion is

located towards the north western part of the study area. This is due to high slope and sparse vegetation and bushes/scrublands, whereas low SER areas were over the high vegetative and lowland area.

4.2. Analysis of classified average annual soil erosion

Classified average annual soil erosion map quantitatively developed using annual soil erosion value is shown in Figure 6. In order to assess the average annual soil loss of Abha watershed these were grouped into five classes based on the minimum and maximum values and the distribution of cell values are showed in Figure 7. The grouping of different soil erosion severity zones was carried out by considering the field conditions.

The results depicted in Table 4, shows that about 89.25% of the total area is classified as very low and low potential SER (<50.00 t h^{-1} y^{-1}), located in eastern and central part of the study area. Whereas, 4.05% classified as high to very high (>100 t h^{-1} y^{-1}) erosion risk levels, and it has been located in north-west and south western part of the watershed. This is due to the denuded slopes that are devoid of forest cover. Herein, the lack of surface cover and the high intensity rainfall is further compounded by the precipitous slopes that result in high soil loss potential in these areas.

4.3. Influence of LULC characteristics on SER

The LULC and SER maps are compared with each other, in this way relationship between the soil erosion and LULC classes may be more clearly analysed and understood. Therefore, the LULC map and the SER map were compared pixel by pixel to generate a table indicating the relationship of the LULC and SER classes, presented in a tabular format. From the LULC of 2010, the high average SER is over the sparse vegetation (54.17 km^2) and bushes and scrublands (36.64 km^2) and it is also noticed that the high SER zone is accounted in sparse vegetation (6.78 km^2) and bushes and scrubland (3.97 km^2).

With the spatial pattern and distribution, high levels of SER zones are distributed over the sparse vegetation, and bushes/scrubland areas (Table 5), which were mostly located in highland areas. However, in flat or almost flat areas, where agriculture is the main land use type, the erosion risk was found to be low. To decrease the SER in sparse forests, scrubland and bushes with limited ground cover should be improved and

Table 4. The ordinal categories of potential annual soil erosion and its area and proportion.

Sl. No.	Numeric range (Mg ha^{-1} y^{-1})	Erosion potential	Area (km)	Proportion (%)
1	0.000–15.00	Very low risk	285.38	77.13
2	15.01–50.00	Low risk	44.85	12.12
3	50.01–100.00	Moderate risk	24.79	6.70
4	100.01–150.00	High risk	8.84	2.39
5	150.01–278.65	Very high risk	6.14	1.66
Total			370	100

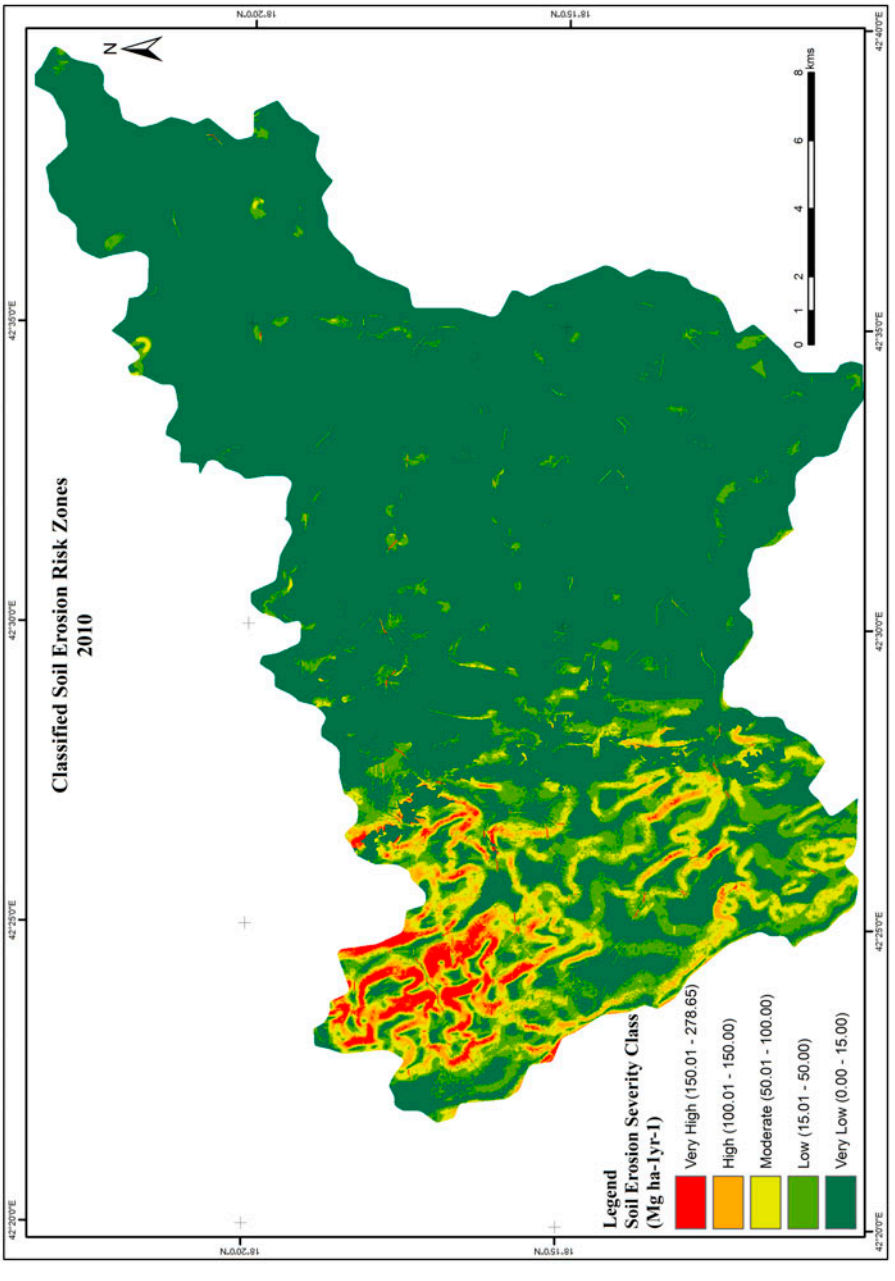

Figure 6. Classified average annual soil erosion.

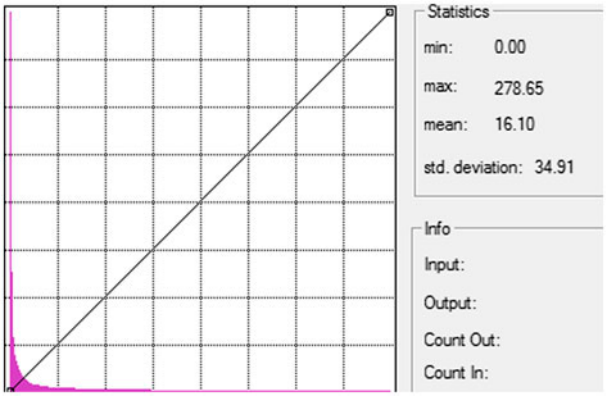

Figure 7. Histogram of soil erosion map.

managed well. Thus, a major part of these lands may be protected from erosion. In addition, the other land covers, such as bare rocks and construction sites, occurred in all risk classes, but few of them had very low risk.

4.4. *Geoaltitudinal analysis of SER*

The area with the larger gradient and covered by high vegetation cover is on lower level of SER. The spatial pattern of annual average SER map shows high spatial correlation with slope map and topography, in controlling soil movement in a watershed. Table 6 indicates that the elevation of > 2550, SER is very high, accounting 5.33 km^2 with mean soil erosion of 50.72–56.62 t h^{-1} y^{-1}. The slope gradiant at this height is high (8.59°–8.72°). The geological unit of this zone are jt (Jiddah Group–Basalt and Andesite–Pillow lava, flow breccia, tuff, dacite tuff, inter-

Table 5. LULC in the semi-arid watershed of Abha with soil erosion statistics.

LULC classes	Mean potential annual soil erosion (Ton/ha/yr)	STD.	VL (0.00–15.00)	*L* (15.01–50.00)	*M* (50.01–100.00)	*H* (100.01–150.00)	VH (150.01–278.65)	Total area
Build-up land	8.93	19.049	30.69	3.58	0.96	0.24	0.10	35.57
Water bodies	0.00	0.000	0.12	0.00	0.00	0.00	0.00	0.12
Agri. Cropland	8.77	16.506	13.10	2.27	0.51	0.04	0.01	15.94
Dense veg.	13.50	31.943	1.72	0.12	0.13	0.06	0.02	2.04
Sparse veg.	54.17	57.157	12.74	9.92	9.17	3.78	3.08	38.69
Fallow land	8.80	16.297	26.15	4.48	1.03	0.09	0.02	31.76
Bare soil/WL	11.18	23.198	12.23	1.70	0.60	0.15	0.08	14.76
Bushes and SL	36.64	45.072	18.69	10.82	7.12	2.54	1.43	40.60
Rock exposed	7.58	24.513	169.97	11.97	5.27	1.94	1.40	190.55
Total			285.41	44.85	24.79	8.84	6.14	370

Note: VL: very low; *L*: low; *M*: moderate; *H*: high; VH: very high

bedded subordinate, often carbonaceous conglomeratic greywacke and phyllie), Oew (Sedimentary–Wajid sandstone) and bt (Jiddah Group–Bahah group within the Tayyah belt – Volcaniclastic greywacke, carbonaceous, shale and siltstone, subordinate chert, slate, and conglomerate, minor interbedded basalt, andesite, and dacite). Whereas, the elevation with low height i.e. 1950–2150 m, SER is very low, accounting 111.76 km^2 with the mean soil erosion of 1.75 t h^{-1} y^{-1}. The slope gradient at this height is very low (1.52°). The geological units of this zone are jt, bt, grb, jbg, mg, and gb. Therefore, the areas with high LS-factor and degraded/sparse vegetation, bushes and scrublands, bare soil/wastelands need immediate attention in soil conservation point of view.

Since the sparse vegetation and bushes and scrubs on hill slopes and denuded hilly areas contribute to the highest potential soil loss in the study area, it is assumed that the rehabilitation of these lands would appreciably ameliorate the soil loss potential from these lands.

4.5. *Altitudinal Impact of LULC on SER*

The high altitudinal mountainous lands are sensitive lands to SER. The topography, with average slope angles between 6° and 12° is favouring surface run-off (USDA, NRCS). The relationship of land use patterns with geophysical were also investigated in this study. For this LULC pattern is arranged with the altitude, slope, rainfall erosivity and geology parameters and their impacts are studied on SER. The analysis shows that the SER over the vegetation cover including dense vegetation, sparse vegetation and bushes/scrubland increases with the higher altitude and higher slope angle. Table 7 indicates that the elevation of 2550–2982 m, SER is very high over sparse vegetation, accounting 27.07 km^2 with mean soil erosion of 60.77–70.68 t h^{-1} y^{-1}. The slope gradient at this height is high (10.71°–11.66°) and the rainfall erosivity is 426–495 MJ mm ha^{-1} h^{-1} y^{-1}. Whereas, the elevation with low height over the sparse vegetation i.e. 1950–2150 m, SER is very low, accounting 6.15 km^2 with the mean soil erosion of 2.21–4.98 t h^{-1} y^{-1}. The slope gradient at this height is very low (1.06°–2.55°) and low rainfall erosivity of 166–173 MJ mm ha^{-1} h^{-1} y^{-1}. This variations are due to slopes-like first hypsometry derivatives, which have strong effect on soil erosion processes. Impermeable lithology, especially schists, which increase surface run-off and allow minimal infiltration and climate plays important role in soil erosion, especially in regard to temperatures and precipitations. Lastly, poorly developed soils (the deepest between 20 and 30 cm), very stony due to the lithology, with minimal organic matter content, fine structure, moderate to low permeability and high percentages of fine sands and silts (see Figure 5) were contributed to high SER. The ideal goal would be to achieve a soil loss rate of 6.7 t ha^{-1} y (Muukkonen et al. 2007; Taguas et al. 2010). This is roughly the rate at which soil can rejuvenate itself.

With the correlation of slope over five LULC types with soil erosion, the response of slope angle variation on soil erosion can be estimated. Spatial statistical analysis of soil erosion with slope angle over different LULC is showed in Table 7 and Figure 8. The statistical analysis suggested that the LULC pattern's slope was strongly related to soil erosion dynamics. Among the LULC pattern, sparse vegetation had higher R^2 values, which reflected that slope angles accelerate the soil erosion (Table 8). Lower slope angle led to decrease in soil erosion formation and transportation. So, the contour

Table 6. Annual mean SER with geoaltitudinal scenario.

Elevation (m)	Slope in degree	Geological units	Mean SER (ton/ha/yr)	Std.	Very low (0.00–15.00)	Low (15.01–50.00)	Moderate (50.01–100.00)	High (100.01–150.00)	Very high (150.01–278.65)	Area
1950–2150	1.52	jt; bt; grb; jbg; mg; gb	1.75	5.14	111.76	1.66	0.19	0.01	0.01	113.64
2151–2350	3.59	dg; jt; bt; grb; jbg	3.38	8.58	124.99	6.40	0.55	0.05	0.04	132.03
2351–2550	7.73	dg; jt; bt; jbg	28.86	37.62	27.48	12.93	8.07	2.43	0.76	51.67
2551–2750	8.59	jt; Oew; bt	50.72	54.24	15.37	16.41	11.03	3.84	3.54	50.18
2751–2982	8.72	jt; Oew; bt	56.62	54.62	5.80	7.45	4.95	2.51	1.79	22.51
Total					285	45	25	9	6	370

Notes: The analysis of soil ersosion with geoaltitudnal effects shows the highest SER is at 2751–2982 of 22.51 area whereas lowest height 1950–2150 indicates low soil erosion with mena of 1.75 and area 113.64 km.
Granite Suite-Biotite Monzogranite-Diorite and Gabbro (dg).
Jiddah Group-Basalt and Andesite-Pillow lava, flow breccia, tuff, dacite tuff, interbedded subordinate, often carbonaceous conglomeratic greywacke and phyllie (jt).
Sedimentary-Wajid sandstone (Oew).
Jiddah Group-Bahah group within the Tayyah belt-Volcaniclastic greywacke, carbonaceous, shale and siltstone, subordinate chert, slate, and conglomerate, minor interbedded basalt, andesite and dacite (bt).
Granite Suite-Biotite Monzogranite-Uniform body (grb).
Jiddah and Bahah group-Biotite-Quartz-Plagioclase Granofels-Subordinate amphibolite, anabiotite schist (jbg).
Dioritic and Gabroic Rocks – Metagabbro (mg).
Dioritic and Gabroic Rocks – Gabbro-Massive to layered plutons, sills, dikes and irregular bodies (gb).

Table 7. Altitudinal impact of LULC pattern on SER.

	Elevation (metres)	Slope in degree	Mean rainfall erosivity	Geological unit	Mean soil erosion	Area in km
Build-up	1950–2150	1.38	173.01	jt, bt, grb, jbg, mg, gb	2.76	10.43
	2151–2350	2.49	162.43	dg, jt, bt, grb, jbg	5.41	20.48
	2351–2550	6.72	276.21	dg, jt, bt	26.78	2.99
	2551–2750	5.8	358.23	jt, bt	30.17	1.26
	2751–2983	6.61	485.75	jt, Oew, bt	41.51	0.61
Agricultural land	1950–2150	1.16	162.5	jt, bt, grb, jbg, mg, gb	1.91	4.62
	2151–2350	2.62	182.8	dg, jt, bt, grb, jbg	4.72	5.51
	2351–2550	6.03	326.39	dg, jt, bt, jbg	25.58	2.32
	2551–2750	7.04	383.6	jt, Oew, bt	33.31	2.13
	2751–2983	8.17	477.79	jt, Oew, bt	38.58	1.36
Dense vegetation	1950–2150	0.71	163.53	jt, bt, grb, jbg, mg, gb	1.23	0.88
	2151–2350	1.92	155.17	dg, jt, bt, grb, jbg	2.61	0.76
	2351–2550	5.69	310.45	jt, bt	16.4	0.04
	2551–2750	9.96	388.07	jt, bt	54.72	0.13
	2751–2983	10.32	485.13	jt, Oew, bt	59.572	0.23
Sparse vegetation	1950–2150	1.06	165.7	jt, bt, grb, jbg, mg, gb	2.21	3.01
	2151–2350	2.55	172.49	dg, jt, bt, grb, jbg	4.98	3.14
	2351–2550	7.98	331.01	dg, jt, bt	41.3	5.47
	2551–2750	10.71	426.4	jt, Oew, bt	60.77	17.25
	2751–2983	11.66	495.55	jt, Oew, bt	70.68	9.82
Bare soil/ wasteland	1950–2150	1.68	163.41	jt, bt, grb, jbg, mg, gb	3.97	10.13
	2151–2350	3.26	191.09	dg, jt, bt, grb, jbg	9.41	2.2
	2351–2550	6.14	335.36	dg, jt, bt	34.1	1.12
	2551–2750	6.61	386.88	jt, bt	31.39	0.73
	2751–2983	6.28	488.2	jt, Oew, bt	32.63	0.58
Bushes and Scrubland	1950–2150	1.25	166.59	jt, bt, grb, jbg, mg, gb	2.28	3.13
	2151–2350	3.11	182.97	dg, jt, bt, grb, jbg	5.22	4.79
	2351–2550	7.74	327.02	dg, jt, bt, jbg	38.74	11.94
	2551–2750	8.64	382.09	jt, Oew, bt	52.79	15.77
	2751–2983	8.64	487.58	jt, Oew, bt	60.12	4.97
Rock outcrop land	1950–2150	1.62	157.32	jt, bt, grb, jbg, mg, gb	1.21	71.48
	2151–2350	4.06	171.89	dg, jt, bt, grb, jbg	2.34	84.28
	2351–2550	8.39	281.93	dg, jt, bt, jbg	22.1	22.2
	2551–2750	7.45	357.02	jt, Oew, bt	45.98	9.85
	2751–2983	7.49	472.78	jt, Oew, bt	54.46	2.79

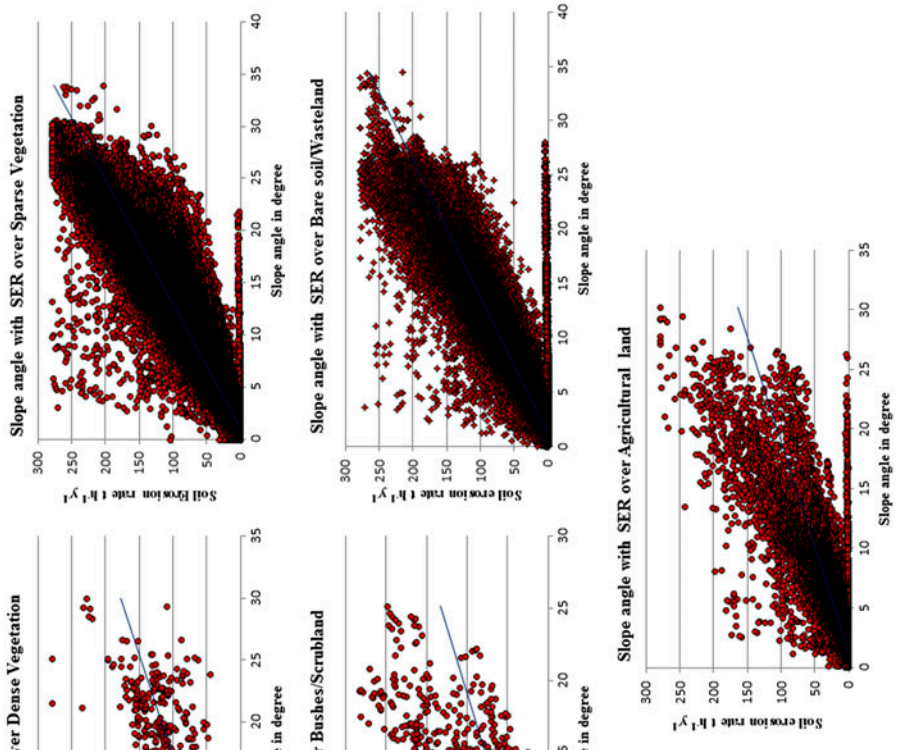

Figure 8. Graphical representation of the relationship between slope angle and soil erosion of LULC patterns.

Table 8. Interaction between slope angle with soil erosion (*S*) of LULC patterns.

Land use/land cover	Dependent	Correlation model	R^2
Dense vegetation	Slope	$S = 6.0625x - 4.4272$	0.8044
Sparse vegetation	Slope	$S = 8.383x - 8.2383$	0.8602
Bushes and scrubland	Slope	$S = 5.4983x - 4.7548$	0.6919
Bare soil/wasteland	Slope	$S = 0.0997x + 2.5289$	0.7944
Agricultural land	Slope	$S = 0.1074x + 2.4457$	0.6081

farming, terracing and higher abundance and distribution of land cover proportion contributed to soil erosion conservation .

5. Conclusion

Soil erosion control, on a specific location, requires a quantitative evaluation of potential soil erosion. In the present research studies, an empirically based 'RUSLE' model integrated with GIS method (considering rainfall, soil properties, LULC, vegetation cover and topography) has been used to predict long-term average annual soil erosion in order to assess the soil erosion intensity to conserve soil and vegetation and rehabilitate vegetation for semi-arid mountainous watershed of Aseer region of Saudi Arabia. The annual average soil erosion rate of the studied watershed is estimated of 16.10 t h^{-1} y^{-1}, due to influences of LULC patterns and topographical variability. It indicates that areas with natural vegetation cover in the head of 'wadies (sub surface water) regions' have minimum rate of soil erosion while areas with human intervention have high rate of soil erosion. The spatial pattern of annual average SER map shows high spatial correlation with slope map and topography, in controlling soil movement in a watershed. Topographical transformation due to anthropogenic activities along with high LS-factor, denuded slope, weak geology (schists and impermeable lithology) and high rainfall intensity to be more susceptible to soil erosion, located in the north-west and south western regions of the study areas. The analysis also shows the SER over the vegetation cover (inclu. dense vegetation, sparse vegetation and bushes/scrubland) increases with the higher altitude and higher slope angle (8–12°). At the higher altitude, the SER is very high over sparse vegetation, accounting 27.07 km^2 with mean soil erosion of 60.77–70.68 t h^{-1} y^{-1} at the slope angle of 10.71°–11.66°. Whereas, at the lower elevation, SER is low, accounting 6.15 km^2 with the mean soil erosion of 2.21–4.98 t h^{-1} y^{-1} at the slope angle of 1.06°–2.55°. This is due to slopes like first hypsometry derivatives, has strong effect on soil erosion processes i.e. with high slope angle. Impermeable lithology, especially schists, which increase surface run-off and allow minimal infiltration and poorly developed soils (the deepest between 20 and 30 cm), very stony due to the lithology, with minimal organic matter content, fine structure, moderate to low permeability and high percentages of fine sands and silts were contributed to high SER. The predicted amount of soil erosion and its spatial distribution can provide a basis for comprehensive management and sustainable land use for the semi-arid mountainous watershed of Abha. The areas located towards the north western and south western part having high and severe SER warrant special attention and priority for the implementation of control measures. While the present analytical model helps mapping of vulnerability zones, micro-scale data on

rainfall intensity, high resolution of DEM data can augment the prediction capability and accuracy of RS and GIS-based SER analysis.

Acknowledgements

The author (Dr Javed Mallick) wish to acknowledge the financial support by Deanship of Scientific Research, King Khalid University, KSA; Project code 62/2012-13. NASA-USGS personnel at the land DAAC provided the latest ASTER-Terra satellite image was also greatly appreciated.

References

Abulfatih HA. 1981. Wild plants of Abha and its surroundings. Saudia Publishing and Distributing House 5: 125–159.

Adediji A, Tukur AM, Adepoju KA. 2010. Assessment of revised universal soil loss equation (RUSLE) in Katsina area, Katsinastate of Nigeria using remote sensing (RS) and geographic information system (GIS). Iranica J Energy Environ. 1:255–264.

Alewell C, Meusburger K, Brodbeck M, Bänninger D. 2008. Methods to describe and predict soil erosion in mountain regions. Landscape Urban Planning. 88:46–53.

Anderson JR, Hardy EE, Roach JT, Witmer RE. 1976. A land use and land cover classification system for use with remote sensor data. Geological survey professional paper 964. Edited by NJDEP, OIRM, BGIA, 1998, 2000, 2001, 2002, 2005.

Angima SD, Stott DE, Neill O, Ong MK, Weesies GA. 2003. Soil erosion prediction using RUSLE for central Kenyan highland conditions. Agric Ecosyst Environ. 97:295–308.

Arnoldus HMJ. 1980. An approximation of the rainfall factor in the universal soil loss equation. In: De Boodt M, Gabriels D, editors. Assessment of erosion. Chichester: Wiley; p. 127–132.

Ayed MG, Adam MA. 2010. The impact of vegetative cover type on runoff and soil erosion under different land uses. Catena. 81:97–103.

Boggs G, Devonport C, Evans K, Puig P. 2001. GIS-based rapid assessment of erosion risk in a small catchment in the wet/dry tropics of Australia. Land Degrad Dev. 12:417–434.

Bonilla CA, Reyes JL, Magri A. 2010. Water erosion prediction using the revised universal soil loss equation (RUSLE) in a GIS framework, central Chile. Chilean J Agric Res. 70:159–169.

Carter MR. 1993. Soil sampling and methods of analysis. Canadian society of soil science. Charlottetown: Lewis Publishers.

Cohen MJ, Shepherd KD, Walsh MG. 2005. Empirical reformulation of the universal soil loss equation for erosion risk assessment in a tropical watershed. Geoderma. 124:235–252.

McCool DK, Foster LC, Mutchler CK. 1989. Revised slope length factor for the universal soil loss equation. Trans ASAE. 32:1571–1576.

Dabral PP, Baithuri N, Pandey A. 2008. Soil erosion assessment in a hilly catchment of North Eastern India using USLE, GIS and remote sensing. Water Resources Management. 22:1783–1798.

Desmet PJJ, Govers G. 1996. A GIS-procedure for the automated calculation of the USLE-LS factor on topographically complex land units. J Soil Water Conserv. 51:427–433.

Dwivedi RS, Sankar TR, Venkataratnam L, Karale RL, Gawande SP, Rao KVS, Senchaudhary S, Bhaumik KR, Mukharjee KK. 1997. The inventory and monitoring of eroded lands using remote sensing data. Int J Remote Sens. 18:107–119.

Fattet M, Fu Y, Ghestem M, Ma W, Foulonneau M, Nespoulous J, Le Bissonnais Y, Stokes A. 2011. Effects of vegetation type on soil resistance to erosion: relationship between aggregate stability and shear strength. Catena. 87:60–69.

Faulkender DJ. 1984. Geological map of the Abha quadrangle, sheet 18F. Kingdom of Saudi Arabia: Saudi Arabian Deputy Ministry for Mineral Resources Geosciences Map GM-75 B, scale 1:250,000

Fernandez LM, Nunez MM. 2011. An empirical approach to estimate soil erosion risk in Spain. Sci Total Environ. 409:3114–3123.

Fu BJ, Zhao WW, Chen LD, Zhang QJ, Lü YH, Gulinck H, Poesen J. 2005. Assessment of soil erosion at large watershed scale using RUSLE and GIS: a case study in the Loess Plateau of China. Land Degrad Dev. 16:73–85.

Gertner G, Wang G, Fang S, Anderson AB. 2002. Effect and uncertainty of digital elevation model spatial resolutions on predicting the topographical factor for soil loss estimation. J Soil Water Conserv. 57:164–182.
Hasan RN, Mallick J, Devi LM, Siddiqui MA. 2013. Multi-temporal annual soil loss risk mapping employing revised universal soil loss equation (RUSLE) model in Nun Nadi Watershed, Uttrakhand (India). Arabian J Geosci. 6:4045–4056.
Hickey R. 2000. Slope angle and slope length solutions for GIS. Cartography. 29:1–8.
Hill J, Schütt, B. 2000. Mapping complex patterns of erosion and stability in dry Mediterranean ecosystems. Remote Sens Environ. 74:557–569.
Hutchinson MF. 1989. A new procedure for gridding elevation and stream line data with automatic removal of spurious pits. J Hydrol. 106:211–232.
Hutchinson MF, Dowling TI. 1991. A continental hydrological assessment of a new grid-based digital elevation model of Australia. Hydrol Processes. 5:45–58.
Knisel WG. 1980. CREAMS: a field scale model for chemicals, runoff, and erosion from agricultural management systems. Utrecht: US Department of Agriculture Research Service, Koninklijk Nederlands Aardrijkskundig Genootschap; 240 p.
Kouli M, Soupios P, Vallianatos F. 2009. Soil erosion prediction using the revised universal soil loss equation (RUSLE) in a GIS framework, Chania, Northwestern Crete, Greece. Environ Geol. 57:483–497.
Lal R. 2001. Soil degradation by erosion. Land Degrad Develop. 12:519–539.
Lee GS, Lee KH. 2006. Scaling effect for estimating soil loss in the RUSLE model using remotely sensed geospatial data in Korea. Hydrol Earth Syst Sci Discuss. 3:135–157.
Li XS, Wu BF, Wang H, Zhang J. 2011. Regional soil erosion risk assessment in Haihe Basin. J Remote Sens. 15:372–387.
Lillesand TM, Kiefer RW. 2000. Remote sensing and image interpretation. 4th ed. New York (NY): Wiley.
Lu GY, Wong DW. 2008. An adoptive inverse-distance weighting spatial interpolation techniques. Comput Geosci. 34:1044–1055.
Lu D, Li G, Valladares GS, Batistella M. 2004. Mapping soil erosion risk in Rondonia, Brazilian Amazonia: using RUSLE, remote sensing and GIS. Land Degrad Dev. 15:499–512
Mallick J, Kant Y, Bharath BD. 2008. Estimation of land surface temperature over Delhi using Landsat ETM+. J Indian Geophy Union. 12:131–140.
Mati BM. 2000. Assessment of erosion hazard with the USLE and GIS: a case study of the upper EwasoNg'iro North basin of Kenya. Int J Appl Earth Observ Geoinf. 2:78–86.
Metternicht GI, Gonzalez S. 2005. FUERO: foundations of a fuzzy exploratory model for soil erosion hazard prediction. Environ Modell Soft. 20:715–728.
Mitasova H, Hofierka J, Zlocha M, Iverson LR. 1996. Modeling topographic potential for erosion and deposition using GIS. Int J GIS. 10:629–642.
Morgan RPC, Quinton JN, Rickson RJ. 1990. Structure of the soil erosion prediction model for the European community. Proceedings of International Symposium on Water Erosion, Sedimentation and Resource Conservation; 1990 Oct 9–13; Dehradun, India: Central Soil and Water Conservation Research and Training Institute, CSWCRTI. p. 49–59.
Muukkonen P, Hartikainen H, Lahti K, Sarkela A, Puustinen M, Alakukku L. 2007. Influence of no-tillage on the distribution and lability of phosphorus in Finnish clay soils. Agr Ecosyst Environ. 120 : 299–306.
Narayana DVV, Babu R. 1983. Estimation of soil erosion in India. J Irrig Drain Eng. 109:419–434.
Nearing MA, Foster GR, Lane LJ. 1989. A process-based soil erosion model for USDA-water erosion prediction project technology. Trans ASAE. 32:1587–1593.
Prasannakumar V, Vijith H, Abinod S, Geetha N. 2012. Estimation of soil erosion risk within a small mountainous sub-watershed in Kerala, India, using revised universal soil loss equation (RUSLE) and geo-information technology. Geosci Front. 3:209–215.
Qinke Y, Rui L, Zhang X, Hu L. 2002. Regional evaluation of soil erosion by water: a case study on the Loess Plateau of China. In: McVicar TR, Rui L, Fitzpatrick R, Changming L, editors. Regional water and soil assessment for managing sustainable agriculture in China and Australia. Melbourne, Australia: ACIAR; p. 304–310.
Renard KG, Foster GR, Weesies GA, McCool DK, Yoder DC. 1997. Predicting soil erosion by water: a guide to conservation planning with the revised universal soil loss equation

(RUSLE). US Department of Agriculture (Editor). Washington (DC): US Department of Agriculture, Agricultural Handbook no 703; p. 1–251
Renschler CS, Flanagan DC. 2002. Implementing a process-based decision support tool for natural resource management: the GeoWEPP example. Trans ASAE. 3: 187–192.
De Roo APJ. 1996. Soil erosion assessment using GIS Geographical information systems in hydrology. Dordrecht: Kluwer Academic Publishers; p. 339–356.
Saha SK, Pande LM. 1993. Integrated approach towards soil erosion inventory for environmental conservation using satellite and agro-meteorological data. Asia-Pac Rem Sens J. 5:21–28.
Shiono T, Kamimura K, Okushima S, Fukumoto M. 2002. Soil loss estimation on a local scale for soil conservation planning. Japan Agric Res Q. 36:157–161.
Taguas EV, Peria A, Ayuso JL, Perez R, Yuan Y, Giraldez JV. 2010. Rainfall variability and hydrological and erosive response of an olive tree micro-catchment under no-tillage with a spontaneous grass cover in Spain. Earth Surf Proc Land. 35 : 750–760.
Wischmeier WH, Smith DD. 1965. Predicting rainfall erosion losses from cropland east of the Rocky Mountains—Guide for selection of practices for soil and water conservation. Washington (DC): US Department of Agriculture (USDA), Agricultural Handbook no 282.
Valor E, Caselles V. 1996. Mapping land surface emissivity from NDVI. Application to European, African and South American areas. Remote Sens Environ. 57:167–184.
Remortel VR, Hamilton M, Hickey R. 2001. Estimating the LS factor for RUSLE through iterative slope length processing of digital elevation data within ArcInfo grid. Cartography. 30:27–35.
Vrieling A. 2006. Satellite remote sensing for water erosion assessment: a review. Catena 65: 2–18
Wang G, Gertner G, Fang S, Anderson AB. 2003. Mapping multiple variables for predicting soil loss by geostatistical methods with TM images and a slope map. Photogrammetric Eng Remote Sens. 69:889–898.
Wischmeier WH, Smith DD. 1978. Predicting rainfall erosion losses – a guide to conservation planning agriculture handbook no 537. Washington (DC): US Department of Agriculture Science and Education Administration; p. 163
Xia A, Clarke KC. 1997. Approaches to scaling of geo-spatial data. In: Quattrochi DA, Goodchild MF, editors. Scale in remote sensing and GIS. Boca Raton (FL): CRC Lewis; p. 309–360.
Yuksel A, Gundogan R, Akay AE. 2008. Using the remote sensing and GIS technology for erosion risk mapping of Kartalkaya Dam watershed in Kahramanmaras, Turkey. Sensors. 8:4851–4865.
Zimmerer KS. 1993. Soil erosion and labor shortages in the Andes with special reference to Bolivia, 1953–1991: implications for “conservation-with-development”. World Dev. 21:1659–1675.